Nanoscale

Accepted Manuscript

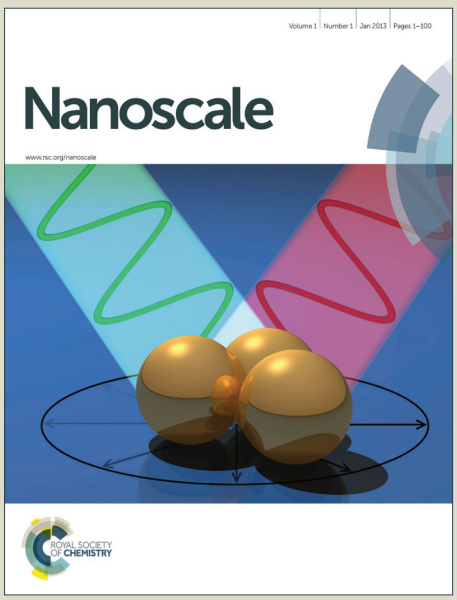

This is an *Accepted Manuscript*, which has been through the Royal Society of Chemistry peer review process and has been accepted for publication.

Accepted Manuscripts are published online shortly after acceptance, before technical editing, formatting and proof reading. Using this free service, authors can make their results available to the community, in citable form, before we publish the edited article. We will replace this *Accepted Manuscript* with the edited and formatted *Advance Article* as soon as it is available.

You can find more information about *Accepted Manuscripts* in the Information for Authors.

Please note that technical editing may introduce minor changes to the text and/or graphics, which may alter content. The journal's standard Terms & Conditions and the Ethical guidelines still apply. In no event shall the Royal Society of Chemistry be held responsible for any errors or omissions in this *Accepted Manuscript* or any consequences arising from the use of any information it contains.

ROYAL SOCIETY OF CHEMISTRY

www.rsc.org/nanoscale

Please do not adjust margins

Journal Name

ARTICLE

Advances in graphene-based semiconductor photocatalysts for solar energy conversion: fundamentals and materials engineering

Received 00th January 20xx,
Accepted 00th January 20xx

DOI: 10.1039/x0xx00000x

www.rsc.org/

Xiuqiang Xie,[a,*] Katja Kretschmer [a] and Guoxiu Wang [a,b*]

Graphene-based semiconductor photocatalysis has been regarded as a promising technology for solar energy storage and conversion. In this review, we summarized recent developments of graphene-based photocatalysts, including preparations of graphene-based photocatalysts, typical key advances of understanding of graphene functions for photocatalytic activity enhancement, methodologies to regulate the electron transfer efficiency in graphene-based composite photocatalysts, by which we hope to offer enriched information to harvest the utmost fascinating properties of graphene as platform to construct efficient graphene-based composite photocatalysts for the solar-to-energy conversion.

1 Introduction

Solar energy conversion by photocatalysis has been attracting much interest as a promising technology for a sustainable future in the context of the aggravating energy and environmental problems such as fossil fuel depletion, pollutions, and global warming.[1, 2] Semiconductor photocatalysis as a promising technique for solar energy conversion has been widely investigated for fuels production, chemical synthesis and environmental remediation.[3] However, photocatalysts still suffer from low quantum efficiency and/or poor stability.[4] Remarkable strides have been made toward increasing the efficiency of solar energy conversion in the past few decades.

Graphene, a two-dimensional sp^2-carbon packed monolayer with exceptional mechanical, thermal, optical, and electrical properties, has been proved to be a promising material in material science and technology.[5] Graphene-based composite materials have evolved into myriad fields ranging from energy storage and conversion,[6] nanoelectronics,[7] optoelectronics,[8] sensors[9] to bio-applications[10-16]. In particular, recent years have witnessed the exploration of graphene-based photocatalysts research with improved solar-to-energy conversion efficiency.[4] Using graphene's springboard, graphene-based semiconductor composite photocatalysts have become a large field of their own.[17-22] Some reviews emerged in the past few years. However, most of the previous reviews mainly focused on the applications of graphene-based photocatalysts. The fundamental science of graphene-based composite photocatalysts is far from being exhausted.[23]

To collect the utmost solar energy, the design of graphene-based photocatalysts at the nanoscale is of particular importance based on the scientific mantra of "structure dictates function" in chemistry.[24] The rational design relies on the fundamentals of photocatalysis over graphene-based photocatalysts, especially the functionalities of graphene for the photocatalytic activity enhancement. However, the comprehensive summary of roles of graphene for the enhanced activity of graphene-based composite photocatalysts has not been available. This situation drives us to summarize recent developments of graphene-based photocatalysts from the points of: i) preparations of graphene-based photocatalysts, ii) typical key advances of understanding of graphene functions for photocatalytic activity enhancement, and iii) methodologies to regulate the electron transfer efficiency in graphene-based composite photocatalysts. This is of importance in order to get a rational and reasonable understanding of this exceptional material.[19] It is hoped that this minireview can be applied as a background source to understand the underlying mechanism of the photocatalytic activity enhancement and harvest the properties of graphene as platform to construct efficient graphene-based composite photocatalysts for solar-to-energy conversion.

1.1 Mechanism and challenges of semiconductor photocatalysts

Figure 1 shows the microscopic reaction pathways of semiconductor photocatalysis, which include three different processes.[25] The reaction is first initiated by light absorption. When semiconductor photocatalysts absorb photons with energy equal to or greater than the band gap ($h\nu \geq E_g$), electrons can be excited from the valence band (VB) to the conduction band (CB), generating highly reactive electrons (e^-) in the conduction band while leaving positive charged holes (h^+) in the valence band (Step I, denoted as S_I in the following discussion). The charge carriers that migrate to the surface of

[a]Centre for Clean Energy Technology, School of Mathematical and Physical Sciences, University of Technology Sydney, Broadway, Sydney, NSW 2007, Australia E-mail: xiexiuqiang@gmail.com, Guoxiu.Wang@uts.edu.au; Fax: 61 2 95141460; Tel: 61 2 95141741
[b]College of Materials Science and Technology, Nanjing University of Aeronautics and Astronautics, Nanjing, P.R. China

Nanoscale Accepted Manuscript

Please do not adjust margins

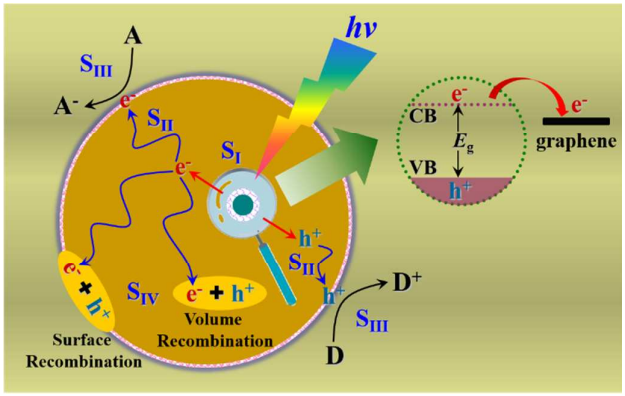

Figure 1. Schematic illustration of photocatalysis over graphene-based composite photocatalysts, in which graphene can enhance the separation efficiency of photogenerated electron-hole pairs, thereby boosting the photoactivity of graphene-based composite toward photooxidation and photoredox reactions.

photocatalysts (Step II, denoted as S_{II}) then participate in the surface oxidation-reduction reactions (Step III, denoted as S_{III}) with the adsorbed reactants: the photo-generated electrons transfer to reduce the adsorbed electron acceptors (A) on the semiconductor surface while the holes oxidize the adsorbed electron donors (D) at a different location, in which the position of the conduction band and the valence band edges determines the reactivity potential of the charge carriers. However, the recombination of charge carriers (Step IV, denoted as S_{IV}), namely the bulk recombination and the surface recombination, takes place predominately (about 90% or more of the photogenerated electrons recombine within 10 ns) as a doom of the electron-hole pairs, which is the key issue that limits the photocatalytic activity and hinders the further development of photocatalysis.[26] Therefore, it is important to increase the lifetime of electron-hole pairs to enhance the photocatalytic activity.

1.2 Why is graphene interesting?

The extraordinary properties of graphene, an allotrope of carbon consisting of one-atom-thick sp^2-hybridized carbon atoms densely packed into a hexagon crystal lattice, have rapidly led the science and technology for low-dimensional nanomaterials into a 2D age. Compared with other allotropes of carbon, *e.g.* diamond, carbon nanotube, and fullerene, this smart sp^2-carbon packed monolayer material possesses varieties of excellent properties, such as high carrier mobility at room temperature (ca. 10000 $cm^2 V^{-1} s^{-1}$),[27] large theoretical specific surface area (2630 $m^2 g^{-1}$),[28] good optical transparency (ca. 97.7%),[29] high Young's modulus (ca. 1 TPa),[30] and excellent thermal conductivity (3000-5000 W $m^{-1} K^{-1}$)[31]. This single-layer hexagonal form of carbon material has been widely employed to improve the catalytic activity of photocatalysts, which can be used as a reservoir for photogenerated-electrons (Figure 1).[32, 33] Because the photogenerated charge carriers are spatially separated, the recombination rate of electrons and holes is reduced and the lifetime of charge carriers is prolonged. Consequently, more oxidative holes and reductive electrons are available for the photocatalytic reactions and the photocatalytic activity is enhanced.

Besides the advantages discussed above, as the platform to design effective photocatalysts, graphene shows exceptional merits, which mainly originate from the synthesis procedure of this versatile carbon material. Since the first reporting of graphene and its manual mechanical cleavage by Scotch tape, several techniques have been developed to obtain this exceptional material. These techniques can be sorted into two categories: bottom-up method and top-down method. The most widely used technique is the Hummers' method[34] or its derivative methods to prepare graphene oxide (GO, the precursor of graphene). By employing this method, graphene can be obtained through the reduction of GO by different strategies, such as hydrothermal reaction,[35] solvothermal reaction,[36] refluxing,[37] and photocatalytic reduction[10, 38-41]. GO can be produced by oxidation of natural graphite powder with strong chemical oxidants followed by exfoliation using ultrasonication or stirring. It is this synthesis procedure that makes graphene superior to its carbon analogues. GO usually possesses a rich assortment of oxygen-containing groups, such as carboxylic, hydroxyl, and epoxide functional groups. On the one hand, these hydrophilic oxygen-containing groups on the surface of GO make it easily dispersible in water, which facilitates the fabrication of graphene-based nanoarchitectures in aqueous solutions.[42] On the other hand, the presence of sufficient oxygen functionalities in GO allows interactions with the cations and serves as reactive sites for the nucleation and growth of nanoparticles, which facilitates the preparation of various graphene-based composites.[43-45] Furthermore, it offers opportunities to tune the surface property of graphene by chemical strategies at the molecular level, such as the grafting of functional groups (amino groups and thiol groups). This chemical tunability of the graphene surface properties will broaden its application for the design of efficient photocatalysts.

Moreover, the particular two dimensional structure of graphene is an attractive option for building efficient diffusion channels of photogenerated-electrons. Photocatalysts could be anchored to both sides of graphene, in other words, more sites can be used to build the interface between photocatalyst and graphene that is vital for electrons transfer. For other carbon materials, for example, one dimensional carbon (carbon nanotubes) or zero dimensional carbon (fullerene), it is relatively hard for photoactive materials to interact with the inner part. In this aspect, graphene holds an unparalleled powerful advantage for the enhancement of photocatalytic activity when compared with its allotropes.

2 Preparation of graphene-based semiconductor photocatalysts

The preparation is of particular importance when building uniform and efficient graphene-based photocatalysts. Metal

Nanoscale Accepted Manuscript

This journal is © The Royal Society of Chemistry 20xx

Table 1. Synthesis of TiO_2/graphene composite photocatalyst

Precursor of graphene	Precursor of TiO_2	Solvent	Additives	Conditions	Morphology feature	Reference
GO powder	P25	H_2O, EtOH	None	Hydrothermal at 120 °C for 3 h	P25 nanoparticle	46
Graphene sheets	Tetrabutyl titanate	EtOH, H_2O	Acetic acid glacial	Stirring for 2 days followed by annealing	TiO_2 nanoparticle	47
GO powder	$TiCl_4$	EtOH, H_2O	None	Sonication for 3 h followed by reduction and calcination	TiO_2 nanoparticle	48
GO solution	$TiCl_4$	H_2O	None	Hydrothermal at 180 °C for 8 h	TiO_2 nanoparticle	35
GO powder	$Ti(BuO)_4$	EtOH, H_2O	H_2SO_4	Stirring at 80 °C for 12 h	TiO_2 nanocrystals	49
Graphene sheets	$Ti(SO_4)_2$	H_2O	H_2SO_4	Hydrothermal at 100 °C	TiO_2 nanospheres	50
GO powder	TiO_2 nanorods	H_2O, Toluene	Oleic acid	Stirring for 24 h at room temperature	TiO_2 nanorods	51
GO powder	Titanium isopropoxide	Benzyl alcohol	Acetic acid	Hydrothermal at 180 °C for 12 h	TiO_2 nanorod	52
GO aqueous suspension	$TiCl_4$	H_2O	None	Hydrothermal at 180 °C for 6 h	TiO_2 nanorod	53
Graphene sheets	TiO_2 powder	H_2O	NaOH, SDS	Hydrothermal	TiO_2 nanotube	54
Colloidal RGO suspension	TiO_2 nanosol	H_2O	None	Reflux at 60 °C for 72 h	TiO_2 nanoplate	37
GO powder	Titanium (IV) (ammonium lactato) dihydroxybis	H_2O and Ethyleneediamine	None	Hydrothermal at 200 °C for 2 h	2D sandwich-like hybrid nanosheets	55
GO solution	Titania nanosheets	H_2O	Polyethyleneimine	Layer-by-layer route followed by UV irridiation	Multilayer hybrid films consisting of alternating graphene and titania nanosheets	56
GO aqueous suspension	$TiCl_4$ & titanium isopropoxide	EtOH or THF	Pluronic P123, polystyrene spheres	Self-assembly at room temperature	Macro-mesoporous TiO_2	57
Nanographe-ne oxides	P25	H_2O	None	Stirring overnight followed by reduction under UV irradiation	P25 core/RGO shell	58
GO aqueous suspension	Titania nanosheets	H_2O	PMMA spheres as templates, PEI	Layer-by-layer assembly followed by microwave irradiation	Hollow spheres consisting of alternating titania nanosheets and graphene	59
GO powder	TiF_4	EtOH, H_2O	None	Hydrothermal at 120 °C for 12 h	High interfacial contact	24
Solvent exfoliated graphene	TiF_4	EtOH, H_2O	Polyvinylpyr-rolidone	Hydrothermal at 120 °C for 12 h	High interfacial contact	60
GO powder	{001}-faceted titania sheet	EtOH, H_2O	None	Microwave-hydrothermal at 180 °C for 1h	{001}-faceted titania sheet	61
GO aqueous suspension	$Ti(SO_4)_2$	EtOH, H_2O	Hydrofluoric acid	Hydrothermal at 180 °C for 16 h	Nanocrystalline TiO_2 with exposed {001} facets	62
GO powder	TiF_4	Butanol	Hydrofluoric acid	Solvothermal at 200 °C for 20 h	TiO_2 nanosheets with exposed {001} facets	63
GO powder	$(NH_4)_2TiF_6$	H_2O	None	Hydrothermal at 160 °C	Graphene@TiO_2 nanocomposites with controlled crystal facets	64

Nanoscale Accepted Manuscript

Please do not adjust margins

GO sheets	TiO_2	H_2O	3-aminopropyltriethoxysilane (APTES)	Stirring at room temperature for 3 h	TiO_2 nanocrystals wrapped by RGO	65
GO	P25	H_2O	None	Hydrothermal at 180 °C for 2 h	TiO_2/graphene hydrogel with 3D interconnected networks	66
GO	Tetrabutyl titanate	Ethanol, Glycerol	None	Hydrothermal at 180 °C	TiO_2 nanowire arrays on graphene	67

oxide, metal sulfide, and metallate semiconductors have been fabricated on graphene in various photocatalytic applications. In this section, the synthesis procedure of semiconductor/graphene composites will be conveyed based on the different types of photocatalysts, with the aim of presenting an obvious guide for the fabrication of graphene-based photocatalysts.

2.1 Synthesis of graphene-based metal oxide photocatalysts

Although a series of metal oxide semiconductors (*e.g.* TiO_2, ZnO, SnO_2, Cu_2O, Fe_2O_3, NiO, and MnO_2) shows promising photocatalytic applications, the most widely studied is still TiO_2. Many preparation protocols have been developed to fabricate TiO_2/graphene composite photocatalysts, as summarized in Table 1. As can be clearly seen, the two most widely used precursors of TiO_2 are either water-dissolvable inorganic titanium salts (*e.g.* $Ti(SO_4)_2$, TiF_4 *etc.*), or titanium alkoxides that can hydrolyze easily in aqueous solution (tetrabutyl titanate, titanium isopropoxide *etc.*). As for the graphene ingredient, GO powder or the aqueous suspension instead of graphene itself is used in most cases. As discussed above, the reason to used GO lies in the fact that the presence of negative charged oxygen moieties on the surface of GO increases the interaction between metal cations and GO and serves as reactive sites for the nucleation and growth of nanoparticles. GO can be readily reduced to graphene *via* hydrothermal/solvothermal process or photocatalysis.[38, 68] If graphene is directly used, for example solvent exfoliated graphene, surfactant such as polyvinylpyrrolidone (PVP) is useful to modify the surface property of graphene to promote the TiO_2 precursor to sufficiently interact with the SEG surface.[60] Furthermore, the morphology of TiO_2 and the interfacial contact between TiO_2 and graphene varies with the preparation conditions.

P25, a mixture of anatase TiO_2 and rutile TiO_2, shows more excellent photocatalytic activity than each single component owing to the nanoscale junction between two crystalline phases. Zhang *et al.* reported that P25 can be anchored onto the surface of graphene *via* a one-step hydrothermal reaction.[46] In the reaction process, GO was reduced to graphene simultaneously with the loading of P25 nanoparticles on the graphene sheet. The presence of a vibration band of Ti-O-C bonds indicated that, during the hydrothermal reduction, GO, with the residual carboxylic acid functional groups, firmly interacted with the surface hydroxyl groups of P25 nanoparticles and finally formed the chemically bonded P25-graphene composites. This is also evidenced by the TEM pictures, which show that there were more P25 particles observed along the edge and wrinkles than on the basal plane since the carboxyl acid groups of GO were likely situated at the edge.[69] However, this tactic severely limits the tunability of the composite properties since one species (P25) is already fixed in the binary composites.

Numerous publications indicate that titanium salts seem to be more suitable for uniformly decorating fine TiO_2 nanoparticles *in situ* on the surface of graphene. Zhang *et al.* prepared particular TiO_2/graphene composites with a sol-gel method using tetrabutyl titanate as the starting materials.[47] It is observed that, for TiO_2/graphene composites, graphene is covered with spherical anatase TiO_2 with sizes from 10 to 15 nm. Using ultrasonication, Guo and co-authors, in a few hours, are successful in a controlled and uniform homogeneous incorporation of TiO_2 nanoparticles on the graphene layers without the use of any surfactant.[48] This means that ultrasound is very effective in dispersing TiO_2 nanoparticles on graphene layers. After calcination, discrete and well-defined TiO_2 fully crystallized particles were uniformly scattered onto graphene sheets. It is also worth noting that by careful control of reaction conditions, Xu *et al.* successfully covered the individual 2D sheet of graphene with TiO_2 semiconductor ingredients fully and intimately *via* one-pot hydrothermal method.[24] In their experiment, the key to achieving this sufficient interfacial contact is to adequately utilize the superior structure-directing role of GO with soluble inorganic salt TiF_4, rather than solid P25, in an aqueous phase.

TiO_2 with different well-defined morphologies has also been constructed on graphene sheets, for example, zero-dimensional TiO_2 nanoshperes, one-dimensional TiO_2 nanorod/nanotube, two-dimensional TiO_2 nanosheet and three-dimensional macro-/meso-porous TiO_2, as summarized in Table 1. In general, those TiO_2 nanoarchitectures can be fabricated and then anchored onto graphene by careful control of the reaction conditions, such as the additives, and hydrothermal parameters, using titanium salts as precursors of TiO_2. Li *et al.* presented a template-free self-assembly process for the direct growth of uniform mesoporous anatase TiO_2 nanospheres on graphene sheets (see Figure 2(a)).[50] According to their report, the epoxy and hydroxyl functional groups on graphene sheets acted as heterogeneous nucleation sites by anchoring anatase TiO_2 nanoparticles, which resulted in the formation of well-dispersed mesoporous anatase TiO_2

Nanoscale Accepted Manuscript

This journal is © The Royal Society of Chemistry 20xx

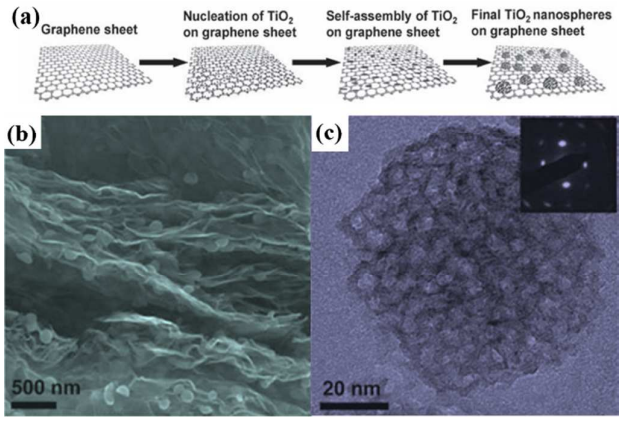

Figure 2. (a) Schematic illustration of the template-free self-assembly strategy for the preparation of mesoporous TiO_2 nanospheres/graphene composites. (b) Side-view of as-prepared mesoporous anatase TiO_2 nanospheres/graphene composites. (c) TEM image of a single mesoporous anatase nanosphere on graphene. The inset in (c) shows the (SAED) patterns related to the whole single nanosphere. Reprinted with permission from ref. 50. Copyright 2011, John Wiley & Sons, Inc.

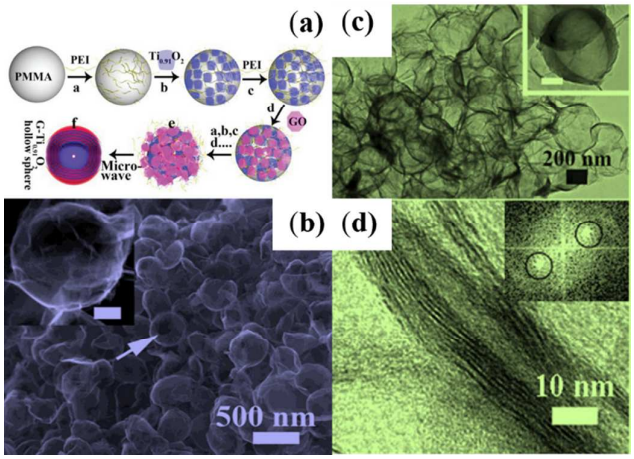

Figure 3. (a) Schematic illustration of procedure for preparing the LBL-assembled multilayer-coated spheres consisting of titania nanosheets and GO nanosheets, followed by microwave reduction of GO into RGO. FESEM images (b), TEM images (c and d) of the hollow spheres. Reprinted with permission from ref. 59. Copyright 2012, John Wiley & Sons, Inc.

nanospheres on the graphene sheets (Figure 2 (b and c)). One-dimensional TiO_2 nanocrystals with small size have large surface area and high quantum size effect, which makes them ideal candidates for photocatalytic and optoelectronic applications. Intrigued researchers prepared TiO_2 nanorods or nanotubes over the entire surface of large graphene sheets.[51-53] For example, as was reported by Liu *et al.*, TiO_2 nanorods stabilized by oleic acid are self-assembled on the GO sheets at the water/toluene interface.[51] The self-assembled GO-TiO_2 nanorod composites can be dispersed in water. The two-phase self-assembling procedure is facile and reproducible, and it can be widely and easily used for self-assembling other nonpolar organic soluble nanocrystals on large GO sheets. TiO_2 nanowire arrays were also grown on graphene substrate by a solvothermal method.[67] During the synthesis procedure, titanium oxyhydrate nanoparticles were bonded on the surface of GO by Ti-O-C bond, which were then transferred to titanium glycerolate (TiGly) in the glycerol-ethanol reaction system. TiGly complexes would gradually grow along the initial nuclei and form the subsequent long nanowire arrays on graphene. TiO_2 powder can be converted to nanotubes under hydrothermal conditions in the presence of NaOH. Zhai *et al.* used a modification of this procedure to produce TiO_2 nanotubes/graphene composites.[54] TiO_2 nanotubes with an average diameter of about 9 nm can hybridize with graphene *via* this method. With the increase of the graphene percentage, graphene sheets covered two sides of TiO_2 nanotubes. Most recently, researchers from Korea reported strongly coupled nanocomposites of layered titanate and reduced graphene oxide (RGO) synthesized by electrostatically derived self-assembly between negatively charged RGO nanosheets and positively charged TiO_2 nanosols, followed bya phase transition of the anatase TiO_2 component into layered titanate. The resultant composite consists of thin 2D nanoplates of lepidocrocite-type layered titanate immobilized on the surface of RGO nanosheets. The composite formation with RGO nanosheets is effective not only in promoting the phase transition of anatase TiO_2 nanosols, but also in improving the thermal stability of the layered titanate, indicating the role of RGO nanosheets as an agent for directing and stabilizing layered structures.[37] Zou's group has prepared TiO_2-graphene 2D sandwich-like hybrid nanosheets by an *in situ* simultaneous reduction-hydrolysis technique in a binary ethylenediamine (En)/H_2O solvent.[55] The technique is based on the simultaneous reduction of GO into graphene by En and the formation of TiO_2 nanoparticles through hydrolysis of titanium (IV) (ammonium lactato) dihydroxybis, resulting in *in situ* loading onto graphene through chemical bonds (Ti-O-C bond) to form a 2D sandwich-like nanostructure. Loh's group from the National University of Singapore have successfully made multilayer hybrid films consisting of alternating graphene and titania nanosheets using layer-by-layer electrostatic deposition followed by UV irradiation.[56] Because titania and GO nanosheets are both negatively charged, positively charged protonic polyethylenimine (PEI) was used as a linker to facilitate the assembly. A layer-by-layer assembly technique has also been used to prepare three-dimensional hollow spheres consisting of alternate titania nanosheets and graphene.[59] In their protocol, as illustrated in Figure 3(a), poly(methyl methacrylate) (PMMA) beads were used as sacrificial templates, while PEI was used as a linker between titania nanosheets and graphene nanosheets. Finally, a microwave irradiation technique was used to simultaneously remove the template and reduce graphene oxide into graphene, and three-dimensional hollow spheres consisting of alternate titania nanosheets and graphene can be obtained (Figure 3(b-d)). As shown in Figure 4(a and b), Geng *et al.* used 3-aminopropyltriethoxysilane (APTES) to modify TiO_2 nanocrystals, producing TiO_2 with positively charged surface.[65] Wrapping GO around TiO_2 nanocrystals was realized by utilizing the electrostatic attraction interaction between the negatively charged GO sheets and the positively charged TiO_2 (Figure 4(c)). After thermal annealing, RGO wrapped TiO_2 nanocrystals were obtained (Figure 4(d and e)). This method

Nanoscale Accepted Manuscript

suppresses the structure directing role of graphene during in-situ processes,[70, 71] thus facilitating the photoactivity tuning of graphene-based composites by changing the geometry of semiconductors.

For nanocrystalline TiO_2, it has been proved by both theoretical and experimental studies that the higher-surface-energy (001) surface has much higher chemical activity and would show greatly enhanced photocatalytic properties with the presence of {001} high energy facets. Research into fabricating high energy {001} facets-exposed nanocrystalline TiO_2 on graphene has also attracted much interest recently. Hydrothermally synthesized TiO_2 nanosheets with exposed (001) facets were *ex-situ* incorporated with graphene by a microwave-assisted hydrothermal treatment.[61] Liu *et al.* and Wang *et al.* developed hydrothermal and solvothermal methods for the synthesis of {001} faceted TiO_2/graphene hybrids separately, during which hydrofluoric acid (HF) was introduced to direct the growth of TiO_2 nanocrystalline.[62, 63] Furthermore, a fluorine-containing titanium salt, $(NH_4)_2TiF_6$, was used as precursor *via* a facile and simple way to synthesize graphene@TiO_2 nanocomposites with controlled crystal facets by a one-pot hydrothermal process.[64] It was found that the concentration of $(NH_4)_2TiF_6$ precursor solutions can also affect the morphologies of graphene@TiO_2 nanocomposites. By control experiments, they found that F^- anions generated by the hydrolysis of $(NH_4)_2TiF_6$ could be preferentially adsorbed into the {001} facets of TiO_2 nanocrystals and limit the growth along the *c*-axis.

Apart from TiO_2, many other metal oxides (*e.g.* SnO_2,[72-74] ZnO,[75-77] Cu_2O,[78] Fe_2O_3,[79] NiO,[80] MnO_2[81] and ZrO_2) have been successfully fabricated on a graphene surface. Compared with that of TiO_2, the procedure to prepare those semiconductor/graphene composites are easier since more water-soluble metal salts can be chosen. As discussed above, the dissociated cations M^{n+} (Zn^{2+}, Sn^{2+}, Cu^{2+}, Fe^{3+}, Ni^{2+}, Mn^{2+} *etc.*) can pre-adsorb on graphene oxide *via* the interaction with negative charged oxygen moieties. Many chemical strategies are then employed to convert these M^{n+}/graphene to M_2O_n/graphene nanocomposites, such as a hydrothermal method,[82] and refluxing[76].

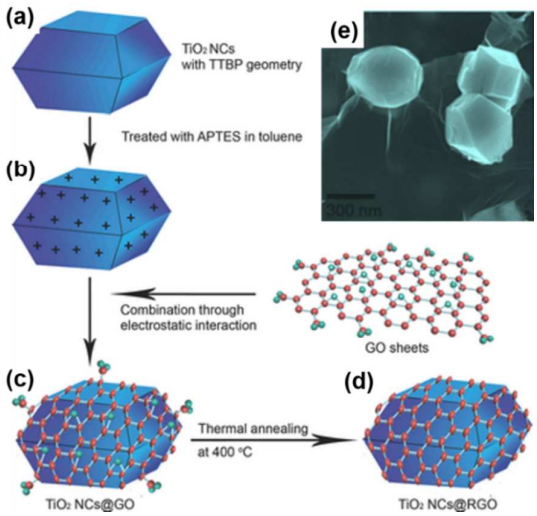

Figure 4. (a-d) Schematic illustration for synthesis of TiO_2 NCs@RGO. (e) SEM image of TiO_2 NCs@RGO. Reprinted with permission from ref. 65. Copyright 2014 WILEY-VCH Verlag GmbH & Co. KgaA, Weinheim.

2.2 Synthesis of graphene-based metal sulfide photocatalysts

Several metal sulfides have been successfully fabricated on graphene sheets, such as CdS,[83-87] In_2S_3,[88] CuS,[89] $ZnIn_2S_4$[90], $Zn_xCd_{1-x}S$,[91] and MoS_2[92]. In summary, two interesting organic compounds were generally employed as sulphur precursor. One was L-cysteine, which is an amino acid that contains three functional groups (-SH, -NH_2, and –COO-) and has a high affinity for cation ions owing to the presence of –SH.[88, 89] L-cysteine can release H_2S when heated, which acts as a sulphur source as well as a reducing agent, resulting in the formation of metal sulfides nanoparticles and the reduction of GO to RGO.[89] It should be mentioned that L-cysteine also plays the role of linker to anchor Cu^{2+} for the well-distributed growth of the CuS nanoparticles on the RGO sheets in their system. The other S-source was dimethyl sulfoxide (DMSO).[83] During the thermal treatment, DMSO can slowly release S^{2-} ions, which is the sulphur source. Furthermore, many metal halides are dissolvable in DMSO, thus it can be used as the solvent directly. Thiourea is another alternative sulphur source that can be used.[87] Like L-cysteine, thiourea can also release H_2S when heated.

Xu *et al.* prepared CdS/graphene composites by a facile solvothermal method in the media of DMSO, during which the formation of CdS nanoparticles and the reduction of GO occur simultaneously.[83] It is found that graphene nanosheets are able to serve as a two-dimensional "mat" with which the CdS nanoparticles interact to hinder the aggregation. By comparing the morphology of CdS/graphene samples with different weight contents of graphene, it is clearly suggested that the introduction of an appropriate amount of graphene to synthesize the CdS/graphene nanocomposite is of great importance for achieving a good and homogeneous distribution of CdS nanoparticles on the two-dimensional graphene scaffold. $Zn_{0.8}Cd_{0.2}S$ was also successfully loaded on RGO by a simple and environmental friendly coprecipitation-hydrothermal strategy using $Cd(Ac)_2{\cdot}2H_2O$, $Zn(Ac)_2{\cdot}2H_2O$, and Na_2S as precursors in the presence of GO.[91] To deposit the solid solution sulfide ($Zn_{0.8}Cd_{0.2}S$) on RGO, aqueous suspension of GO was added into the mixture of $Cd(Ac)_2{\cdot}2H_2O$ and $Zn(Ac)_2{\cdot}2H_2O$ in water. After that, Na_2S solution was added dropwise followed by stirring for 2 h at room temperature. The suspension was then hydrothermally treated at 160 °C for 4 h and $Zn_{0.8}Cd_{0.2}S$/RGO composites were obtained after washing and drying. Wu and co-authors deposited *p*-type MoS_2 nanoplatelets on the *n*-type nitrogen-doped reduced graphene oxide (*n*-RGO) nanosheets by a solvothermal method at 200 °C for 10 h using $(NH_4)_2MoS_4$, L-ascorbic acid and GO dispersed in N, N-dimethylformamide (DMF) as starting materials.[92] The p-MoS_2/n-RGO heterostructure shows significant photocatalytic activity toward the hydrogen evolution reaction (HER) in the wavelength range from the ultraviolet light through the near-infrared light.

Nanoscale Accepted Manuscript

This journal is © The Royal Society of Chemistry 20xx

2.3 Synthesis of metallate/graphene composite photocatalysts

Many other semiconductor photocatalysts have been constructed on graphene, such as Bi_2WO_6,[93, 94] $BiVO_4$,[95] γ-Bi_2MoO_6,[96, 97] $Sr_2Ta_2O_7$,[98] $ZnFe_2O_4$,[99] $MnFe_2O_4$,[100] $CoFe_2O_4$,[101] BiOBr,[102, 103] BiOI,[104] $Bi_5Nb_3O_{15}$,[105] $La_2Ti_2O_7$,[106] $ZnWO_4$,[107] and $InNbO_4$[108]. Most preparations of these metallate/graphene composites are conducted under hydrothermal conditions. Some composite photocatalysts are prepared by a one-step hydrothermal method. Fu *et al.* used $Co(NO_3)_2{\cdot}6H_2O$ and $Fe(NO_3)_3{\cdot}9H_2O$ as precursors of $CoFe_2O_4$, and GO as a source of graphene sheets.[101] During the hydrothermal reaction process, GO was reduced to graphene, and simultaneously $CoFe_2O_4$ nanoparticles were formed on the graphene sheets. $CoFe_2O_4$ nanoparticles have a magnetic property, which makes the $CoFe_2O_4$/graphene composite magnetically separable in a suspension system, and therefore it does not require additional magnetic components as is the usual case. Other magnetically separable materials such as $MnFe_2O_4$,[100] and $ZnFe_2O_4$,[99] were also fabricated on graphene by the same method. The one-step hydrothermal method can be also successfully used for the synthesis of Bi_2WO_6,[93, 94] $BiVO_4$,[95] and γ-Bi_2MoO_6[97] loaded graphene composites. Ye *et al.* reported the synthesis of Bi_2WO_6/RGO composites by an *in situ* reaction.[94] In a typical experiment, $Na_2WO_4{\cdot}2H_2O$, $Bi(NO_3)_3{\cdot}6H_2O$ and GO (dispersed in water) were added successively into distilled water under vigorous stirring followed by 30 min ultrasonication, sodium alginate solution was added slowly. After being stirred for 3 h, the suspension was sealed in a Teflon-lined autoclave and maintained at 180 °C for 16 h. Bi_2WO_6/RGO composites were obtained after washing and drying processes. Bi_2MoO_6/RGO composite photocatalysts have been successfully fabricated by a one-pot solvothermal method.[97] The Bi-precursor $Bi(NO_3)_3{\cdot}5H_2O$ was dissolved in ethylene glycol, which was mixed with GO dispersed in ethylene glycol under vigorous stirring. After that, $Na_2MoO_4{\cdot}2H_2O$ as the Mo-precursor was added to the mixture to form a suspension, which was hydrothermally treated at 160 °C for 12 h before Bi_2MoO_6/RGO composite formed. In other cases, semiconductor nanoparticles are prepared and incorporated with graphene by *ex situ* integration method in different conditions.[102-108] A simple surface charge modified self-assembly approach was applied to prepare two-dimensional (2D) $SnNb_2O_6$ nanosheet/graphene composites featuring a typical 2D-2D structure.[109] After the reduction of GO by branched polyethylenimine (BPEI) through refluxing, modified graphene nanosheets with a positively charged surface can be obtained. The electrostatic attractive interaction between negatively charged $SnNb_2O_6$ nanosheets and positively charged graphene in an aqueous solution enables the efficient self-assembly process to prepare the $SnNb_2O_6$/graphene composites with sheet-on-sheet structure. Liu *et al.* reported GO enwrapped Ag_3PO_4 composite as a visible-light-induced photocatalyst fabricated through an ion-exchange method of CH_3COOAg and Na_2HPO_4 in the presence of GO sheets, which could serve as a support and surfactant to enwrap Ag_3PO_4 particles.[110]

3 Functions of graphene for photocatalytic activity enhancement

Graphene-based semiconductor photocatalysts show wide applications, such as environmental remediation[32, 46, 87], organic synthesis[55, 59, 60, 83, 84, 111] and water splitting[47, 53, 78, 86, 112, 113]. Besides the effort to combine graphene with semiconductor photocatalysts to enhance their photocatalytic performance, numerous attempts have been made to reveal the origin of the activity enhancement, which in turn provides fundamental science to construct graphene-based semiconductor photocatalysts with higher photoactivities. This section will discuss recent advances regarding the functions of graphene for photocatalytic activity enhancement.

3.1 Enhanced adsorptivity for reactants

Surface adsorption is a prerequisite for photocatalytic processes. A previous report showed that the graphene/rod-shaped TiO_2 nanocomposite samples with high BET surface area exhibit higher photocatalytic performance toward the degradation of methyl orange (MO) than P25 as well as pure rod-shaped TiO_2 nanocrystals.[52] The enhanced physical adsorption of molecules, owing to the higher BET surface contributes to the photoactivity improvement. Zhang *et al.* found that there were no significant changes in the BET specific area among the three catalysts, though the adsorption strength P25 decorated graphene composite (P25/graphene) is better than that of bare P25 and P25/carbon nanotubes (P25/CNTs), as shown in Figure 5(a), which indicated that the adsorptivity should not merely originate from simple physical adsorption.[46] The enhanced adsorptivity should be largely

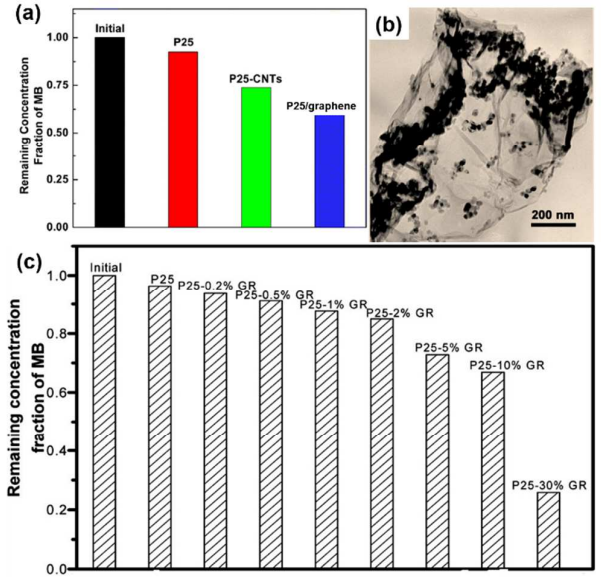

Figure 5. (a) Bar plot showing the remaining methylene blue (MB) in solution in the dark after 10 min stirring. (b) Typical TEM image of P25-graphene, with P25 loading on the surface of graphene and concentrating along the wrinkles.[46] (c) Bar plot showing the remaining methylene blue in solution after reaching the adsorption equilibrium in the dark over the P25-GR nanocomposites.[32] Reprinted with permission from ref. 46 and 32. Copyright 2009, American Chemical Society.

Nanoscale Accepted Manuscript

assigned to the selective adsorption of the aromatic dye on the catalyst. Since the basal graphene plane was not fully covered by P25 (Figure 5(b)), it is reasonable to conclude that the adsorption was noncovalent and driven by the π-π stacking between methylene blue (MB) and aromatic regions of the graphene, which was similar to the conjugation between aromatic molecules and CNTs. In addition, the P25-graphene showed better adsorption of MB than P25-CNTs mainly owing to its giant π-conjugation system and two-dimensional planar structure, and therefore exhibited faster photodegradation of the dyes. However, this work did not consider the effect of different addition ratios of graphene into the matrix of TiO_2 on changing of the photocatalytic activity of TiO_2. Xu *et al.* prepared a series of P25-graphene (P25-GR) composites with different graphene addition ratios and demonstrated that with the increase of graphene in the P25-GR nanocomposites, the adsorption of methylene blue increases correspondingly (Figure 5(c)).[32] This can be ascribed to the increased exposure of graphene in the composite, resulting in the favorable π-π interactions between methylene blue and graphene.

The adsorption behavior of reactants over graphene-based semiconductor photocatalysts depends critically on the coupling pattern between semiconductors and graphene. Xu *et al.* prepared CdS/graphene composites (CdS/GR) by a facile solvothermal method (Figure 6(a)) and found that, although CdS/GR composite exhibited much improved photocatalytic activity toward the selective oxidation of aromatic alcohols, the adsorption capacity for aromatic alcohols over the CdS/GR composite is almost the same as for blank-CdS, as shown in Figure 6(b).[83] This may be attributed to the shielding effect of CdS that caused the graphene surface to be densely covered by the CdS component (Figure 6(c)). As a result, the interaction between aromatic alcohols and graphene *via* π-π stacking is spatially blocked and no obvious adsorptivity improvement was observed.

3.2 Extended light absorption range

Light absorption is of importance since photocatalysis is initiated by photo excitation. Many reports indicate that graphene is able to extend the light absorption range of semiconductors. One possible underlying mechanism may be surface carbon doping because of the chemical bonding between semiconductor and graphene.[84] The surface carbon doping effect of graphene often leads to the light absorption edge extension of TiO_2 from ultraviolet range to visible range, thus making TiO_2/graphene composite a visible-light-response photocatalyst. As reported by Li *et al.*,[46] Ti-O-C vibration absorption band was observed in their Fourier transform infrared (FT-IR) spectra and an obvious red shift of ca. 30-40 nm in the absorption edge of P25-graphene powder, compared with bare P25, which is similar to the case of carbon doped TiO_2 composites[114]. Ti-O-C is also observed in other reports, which can extend the photo-response from ultraviolent region to visible light region.[48, 54, 61, 115-118]

Besides the TiO_2/graphene system, an extension of light absorption range was also observed in the CdS/graphene system. It was reported that the band gap of the

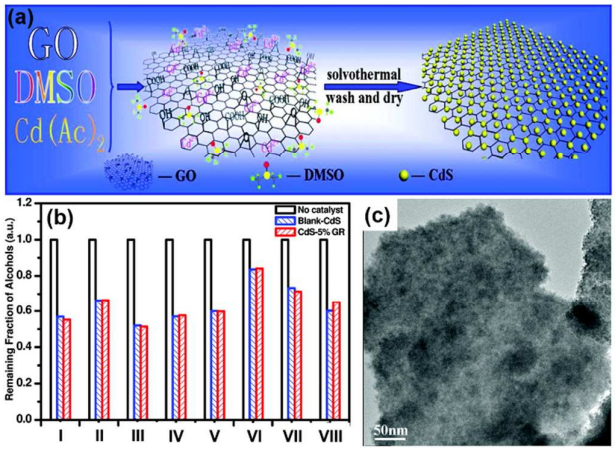

Figure 6. (a) Solvothermal preparation of CdS/GR composites. (b) Remaining fraction of various alcohols after the adsorption-desorption equilibrium is achieved over blank-CdS and CdS/GR composites: (I) benzyl alcohol; (II) p-methylbenzyl alcohol; (III) p-methoxybenzyl alcohol; (IV) p-nitrobenzyl alcohol; (V) p-fluorobenzyl alcohol; (VI) p-chlorobenzyl alcohol; (VII) cinnamyl alcohol; (VIII) 3-methyl-2-buten-1-ol. (c) Results of HRTEM for CdS/GR composites. Reprinted with permission from ref. 83. Copyright 2011, American Chemical Society.

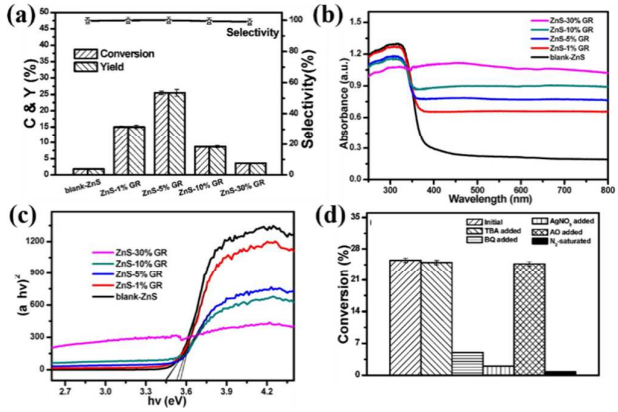

Figure 7. (a) Results of photocatalytic selective oxidation of benzyl alcohol over blank ZnS and ZnS/GR nanocomposites under visible light irradiation (λ > 420 nm) for 4 h. (b) UV–visible diffuse reflectance spectra (DRS) of the samples of ZnS–GR nanocomposites with different weight addition ratios of graphene. (c) The plot of transformed Kubelka-Munk function *versus* the energy of light. (d) Controlled experiments of photocatalytic selective oxidation of benzyl alcohol in the presence of *tert*-butyl alcohol (TBA, scavenger for hydroxyl radicals), benzoquinone (BQ, scavenger for superoxide radicals), $AgNO_3$ (scavenger for electrons), ammonium oxalate (AO, scavenger for holes), or N_2-saturated condition over the optimum ZnS–5% GR for 4 h under visible light irradiation (λ > 420 nm).[111] Reprinted with permission from ref. 111. Copyright 2012, American Chemical Society.

semiconductor CdS is narrowed owing to the introduction of graphene into the matrix of CdS/graphene nanocomposites because of the chemical bonding between CdS and graphene.[83] Based on the Kubelka-Munk function versus the energy of light, the estimated band gap values of the samples are about 2.46, 2.43, 2.34, 2.33, and 2.24 eV approximately, corresponding to blank-CdS, CdS-1% graphene, CdS-5% graphene, CdS-10% graphene, and CdS-30% graphene nanocomposites, respectively. Such a similar phenomenon of band gap narrowing has also been observed for ZnS/graphene nanocomposites.[111]

Nanoscale Accepted Manuscript

This journal is © The Royal Society of Chemistry 20xx

3.3 Photosensitizer/Photon-absorber

The above results showed that graphene addition may lead to band gap narrowing of the semiconductor owing to the chemical bonding between semiconductor and graphene, which results in the extended light absorption range. It is also worth noting that recent large-scale density functional calculations on the model of the graphene/TiO_2(110) interface, along with the experimental proof from the wavelength-dependent photocurrent study, have suggested the possible role of graphene as a photosensitizer for TiO_2.[119] The new role of graphene as the sensitizer opens a promising wide scope to exploit the potential applications of graphene-based semiconductor. However, experimentally, the photocurrent measurement alone cannot be sufficient to prove whether or not graphene acts as a photosensitizer for a semiconductor during a photocatalytic process for the graphene/TiO_2(110) system, since this work does not exclude the effect of a Ti-O-C bond being formed between TiO_2 and graphene, that is, surface carbon doping which leads to the light absorption edge extension of TiO_2 from ultraviolet range to visible range. Xu's group confirmed by detailed experiments the role of graphene in the ZnS/graphene (ZnS/GR) nanocomposites as an organic dye-like macromolecular "photosensitizer" for ZnS instead of an electron reservoir.[111] It was found that ZnS/GR nanocomposites exhibit visible light photoactivity toward aerobic selective oxidation of alcohols and epoxidation of alkenes under ambient conditions, as exemplified in Figure 7(a). However, ZnS by itself shows very poor photoactivity towards the oxidation of benzyl alcohol. Unlike the TiO_2/graphene system, as indicated in Figure 7(b and c), the optical measurement of ZnS/GR indicates that the wide band gap of ZnS is narrowed to some degree, but still not enough for the visible light region. Consequently, it can be inferred that graphene may act as a visible light photosensitizer to ZnS in the nanocomposite of ZnS/GR. In other words, under visible light irradiation, photoexcited electrons are generated from graphene and then transferred to the conduction band of ZnS, which therefore transforms the wide band gap ZnS to a visible light photocatalyst. The controlled experiments using different radicals scavengers shown in Figure 7(d) support the inference on the role of graphene as a macromolecular organic dye-like photosensitizer to ZnS for ZnS-5% GR. It is interesting to note that the addition of ammonium oxalate (AO) scavenger for holes has a negligible effect on conversion of benzyl alcohol, thus indicating holes do not involve the oxidation of benzyl alcohol. This result is in accordance with the proposed photocatalytic mechanism that graphene acts as a visible light photosensitizer in ZnS-5% GR during which no holes are generated because ZnS cannot be band-gap-photoexcited by visible light irradiation. When $AgNO_3$ scavenger for electrons is added, conversion of substrate reactants is remarkably inhibited. Similarly, the addition of benzoquinone (BQ) scavenger for superoxide radicals also significantly prohibits the conversion. Besides, a controlled experiment in inert N_2-saturated atmosphere implies that only trace conversion is obtained. Thus, these controlled experiments suggest that (i) oxygen is the primary oxidant in our photocatalytic oxidation system, and (ii) photocatalytic oxidation of alcohols or alkenes over ZnS-5% GR under visible light irradiation can be understood by a graphene-induced photosensitization process.

Graphene also exhibits strong near-infrared (NIR) absorbance and was applied for NIR photothermal therapy of cancer.[15, 120] Akhavan *et al.* developed a magneto-photothermal therapy for cancer using superparamagnetic zinc ferrite spinel ($ZnFe_2O_4$)-RGO nanostructures (with various RGO contents).[15] *In vitro* application of a low concentration (10 μg mL^{-1}) of the $ZnFe_2O_4$–RGO (20 wt%) nanostructures under a short time period (~1 min) of NIR irradiation (with a laser power of 7.5 W cm^{-2}) resulted in an excellent destruction of the prostate cancer cells, in the presence of a magnetic field (~1 Tesla) used for localizing the nanomaterials at the laser spot. The reported results may stimulate more applications of magnetic graphene-containing composites in highly efficient photothermal therapy.

3.4 Electron transfer mediator

The calculated Fermi level (E_F) of graphene is -0.08 V versus NHE, which is more positive than the E_{CB} of most semiconductors.[93, 121] Consequently, photogenerated electrons will spontaneously transfer from semiconductors to graphene nanosheets when they come into contact. Furthermore, graphene has a high charge-carrier mobility of 250000 cm^2 V^{-1} s^{-1} at room temperature, so electrons can transfer in the network of graphene with ease and unconstrained. Based on these two features, the most widely acceptable role of graphene for photocatalytic activity enhancement is as the electron transfer mediator, *i.e.*, photo-generated electrons from a semiconductor will thermodynamically migrate to graphene, where they are then captured by electron-acceptors. Consequently, the electron-hole pairs separation rate can be significantly enhanced.

In an ideal system, quantum yield (ϕ), which indicates the efficiency of the photocatalytic process, is proportional to the following relationship:

$$\phi \propto k_{CT}/(k_{CT} + k_R)$$

where k_{CT} is the rate of the charge transfer processes and k_R indicates the electron-hole recombination rate (both bulk and surface). The above relationship between ϕ and k_R indicates that graphene can enhance the photocatalytic efficiency by reducing the recombination of electron-hole pairs.[122] The electrons transferred to graphene are consumed by miscellaneous acceptors, which increase the photocatalytic performances toward different applications. On the one hand, photo-excited electrons from semiconductors to graphene can be further transferred to surface adsorbed O_2 by either one-electron transfer process to form superoxide radical species or two-electrons transfer process to form H_2O_2[123], which can be used for the selective transformation of alcohols to the corresponding aldehydes or environmental remediations.[20] On the other hand, the spatially separated excited electrons can directly reduce the nitro compounds adsorbed on graphene,[124]

Nanoscale Accepted Manuscript

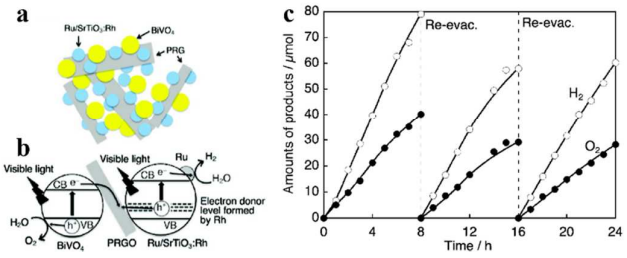

Figure 8. (a) Schematic image of a suspension of $Ru/SrTiO_3$ and $PRGO/BiVO_4$ in water at pH 3.5. (b) Mechanism of water splitting in a Z-scheme photocatalysis system consisting of $Ru/SrTiO_3$:Rh and $PRGO/BiVO_4$ under visible-light irradiation. (c) Overall water splitting under visible-light irradiation by the ($Ru/SrTiO_3$:Rh)–($PRGO/BiVO_4$) system. Conditions: catalysts (0.03 g each) in H_2SO_4(aq) (pH = 3.5, 120 mL); light source, 300 W Xe lamp with a 420 nm cutoff filter; top-irradiation cell with a Pyrex glass window.[125] Reprinted with permission from ref. 125. Copyright 2011, American Chemical Society.

or H^+ to realize photocatalytic H_2 production[22]. In addition, Wu *et al.* reported the preparation of α-Fe_2O_3/graphene composites for photocatalytic water oxidation.[126] Investigations show that electron transfer to the graphene could increase the charge separation and suppress the charge recombination, leaving long-lived holes in the α-Fe_2O_3 to oxidize water, increasing the photocatalytic water splitting rate.

The improved electron-hole separation efficiency by graphene can also lead to enhanced photocatalytic performances in biology, such as antibacterial,[10, 16] antiviral,[11] anti-parasitical applications,[12] and photostimulation of stem cells[13, 14]. Akhavan's group conducted extensive investigations on the bio-applications of graphene-based composite photocatalysts. For example, they prepared TiO_2/RGO thin films by depositing GO onto the TiO_2 thin films followed by calcination.[10] The TiO_2/RGO thin films exhibited enhanced performance for the degradation of Escherichia coli bacteria compared to bare TiO_2 films. Moreover, as a result of the electron transfer from TiO_2 to RGO, the residual oxygen-containing functional groups on RGO can be reduced by the accumulated photo-excited electrons. Vertical aligned ZnO nanowires and WO_3 have been also successfully integrated with graphene for the visible-light photo-inactivation of bacteria[16] and bacteriophage MS2 viruses[11] with enhanced photocatalytic performance. RGO sheets deposited on a TiO_2 film worked as a biocompatible layer for accelerated neuronal differentiation of human neural stem cells (hNSCs) in the presence of a biocompatible hole scavenger.[12] The effective electrical coupling between the TiO_2 and the RGO, through the Ti-C and Ti-O-C bonds formed in the TiO_2/RGO composites, as well as between the RGO sheets and hNSCs provided not only more proliferation of the cells (by a factor of ~2.5) but also more differentiation of hNSCs into neurons than glia (in total, ~23-fold increase in neural to glial cell ratio), under flash photo stimulation. Furthermore, Akhavan *et al.* proceeded to incorporate TiO_2 with graphene nanogrids for the differentiation of human neural stem cells into neural networks.[13] A higher differentiation on the reduced graphene oxide nanoribbon (RGONR) grids than RGO sheets was observed, which can be assigned to the physical stress induced by the surface topographic features of the nanogrids.

Because of its large two-dimensional mat-like structure with a size of several micrometers, the possibility of using graphene as the conductive medium to interface the H_2 and O_2 photocatalysts was explored, and it was found that perfectly interpreted its function as an interparticulate electron transfer mediator.[125] In the report, the effectiveness of reduced graphene oxide as a solid electron mediator for water splitting in the Z-scheme photocatalysis system is demonstrated. As illustrated in Figure 8(a and b), a tailor-made, photoreduced graphene oxide can shuttle photogenerated electrons from an O_2-evolving photocatalyst ($BiVO_4$) to a H_2-evolving photocatalyst ($Ru/SrTiO_3$:Rh), tripling the consumption of electron-hole pairs in the water splitting reaction under visible-light irradiation (Figure 8(c)). This work has paved a new way of using the attractive graphene in the design of new and efficient systems for water splitting. Lu *et al.* also demonstrated that graphene can play an important role as an electron transfer highway, which facilitates the charge carrier collection onto Pt cocatalysts. The quantum efficiency for $Sr_2Ta_2O_{7-x}N_x$ with Pt cocatalyst in the wavelength of 280-550 nm was calculated to be 4.26%. This value was further improved to 6.45% (~177% increase compared with the value of 2.33% for undoped $Sr_2Ta_2O_7$) when Pt-loaded graphene scaffolds were incorporated into the $Sr_2Ta_2O_{7-x}N_x$ photocatalyst.[98]

The role of graphene as an efficient electron transfer enables the prolonged stability of photocatalysts, such as ZnO,[127-130] Ag_3PO_4[131] and plasmonic Cu[132]. Ag_3PO_4, a highly efficient photocatalyst for O_2 generation from water splitting and organic dyes degradation under visible light irradiation, suffers poor cyclability because of photocatalytic reduction of Ag^+ to Ag. The work by Yang and co-authors demonstrated that the transfer of photogenerated electrons from the surface of Ag_3PO_4 to graphene sheets also reduces the possibility of decomposing Ag^+ to metallic Ag, promising an improved stability of recyclable Ag_3PO_4-graphene composite photocatalyst.[131] Copper is a low-cost plasmonic metal, which can gain visible light energy through the localized surface plasmon resonance (LSPR) effect to improve the yield of photocatalytic chemical synthesis. Although Cu nanoparticles exhibit strong LSPR absorption in the visible light range and are catalytically active for many reactions such as the catalytic hydrogenation of dimethyl oxalate, the primary challenge for Cu nanoparticles to be used as photocatalyst is their chemical stability under catalytic reaction conditions. Cu nanoparticles are easily oxidized to Cu_2O or CuO in air or in the presence of traces of molecular oxygen. Recent investigations suggest that graphene can be used as support to stabilize Cu nanoparticles susceptible to oxidation, which are feasible for igniting and promoting the coupling reactions of aromatic nitro compounds to corresponding azoxy or azo compounds under visible-light irradiation.[132] This work may lead to the revisiting of this low-cost plasmonic metal as photocatalyst for solar energy conversion.

Nanoscale Accepted Manuscript

This journal is © The Royal Society of Chemistry 20xx

4 Materials engineering towards improving the electron transfer efficiency in graphene-based photocatalysts

To harness the role of graphene as electron transfer mediator, the optimization of interfacial electron transfer from semiconductors to graphene and the electron transfer within graphene by rational material design deserves more effort, which will ultimately enhance the quantum efficiency of graphene-based semiconductor photocatalysts.

Xu and co-workers conceptually proved that TiO_2/graphene composites with intimate interfacial contact exhibit significantly higher visible light photoactivity toward selective oxidation of alcohols than their counterpart with poor interfacial contact, which paves the way for enhancing the performance of graphene-based semiconductor photocatalysts by interfacial electron transfer engineering.[24] Zeng *et al.* have recently prepared chemically bonded TiO_2/graphene through the Ti-C bond, which could provide a good spatial condition for charge transport from TiO_2 to graphene *via* the interfaces, and decrease the possibility of the recombination of electron−hole pairs, and thus lead to higher photocatalytic activity towards photodegradation of formaldehyde in air.[133] Additionally, Xu *et al.* showed a proof-of-concept study on improving the photocatalytic performance of TiO_2/graphene nanocomposites *via* a combined strategy of decreasing defects of graphene and improving the interfacial contact between graphene and the semiconductor TiO_2.[60] The solvent exfoliated graphene (SEG) in N, N-dimethyl-formamide (DMF) has much lower defects density, which endows SEG with the improved electrical mobility and a longer electronic mean free path. This decreases the likelihood of the recombination of photogenerated electron-hole pairs in the SEG-P25 nanocomposite upon light irradiation.[134] The utilization of SEG instead of GO as the precursor of graphene along with strengthening interfacial contact between TiO_2 and the graphene surface is a feasible approach to improve the photocatalytic performance of TiO_2/graphene. It enables the sufficient harnessing of the electron conductivity of graphene to achieve a more efficient TiO_2/graphene nanocomposite with enhanced photoactivity for the synthesis of fine chemicals by selective oxidation under ambient conditions.

A more encouraging work by Xu *et al.* demonstrated a simple and general approach to improve the transfer efficiency of photogenerated charge carriers across the interface between graphene and semiconductor CdS by introducing a small amount of metal ions (Ca^{2+}, Cr^{3+}, Mn^{2+}, Fe^{2+}, Co^{2+}, Ni^{2+}, Cu^{2+}, and Zn^{2+}) as "mediator" into their interfacial layer matrix, while the intimate interfacial contact between graphene and CdS is maintained (Figure 9(a)). Metal ions as generic interfacial mediator can significantly improve the visible-light-driven photoactivity of CdS/graphene (CdS/GR) semiconductor composites for targeting selective photoredox reaction, including aerobic oxidation of alcohol (Figure 9(b)). Without the presence of metal ions as interfacial mediators in the composites, CdS-GR with 5% graphene exhibited the optimum efficiency for the selective conversion of benzyl alcohol. In contrast, for the optimal CdS-(GR-M) photocatalysts, the weight addition ratio of graphene is remarkably increased to 10 or 30%. This suggests that the metal ions as interfacial mediators can also drive a balance between the positive effect of graphene on retarding the recombination of electron-hole pairs photogenerated from semiconductor and the negative "shielding effect" of graphene as a result of the high weight addition of graphene.[135] As evidenced by photoluminescence spectra shown in Figure 9(c), the introduction of metal ions as interfacial mediator between graphene and CdS can significantly optimize the charge carrier transfer pathway across the interface between CdS and graphene and thus prolong the lifetime of photogenerated charge carriers. As a result, the negative shielding effect of a higher amount of graphene can be counterbalanced effectively and the photoactivity of CdS/GR is significantly improved. Figure 9(d) shows the electrochemical impedance spectroscopy (EIS) Nyquist plots of a series of electrodes. As compared to blank CdS, the optimal CdS-(GR-M) (M = Ca^{2+}, Cr^{3+}, Mn^{2+}, Fe^{2+}, Co^{2+}, Ni^{2+}, Cu^{2+}, and Zn^{2+}) electrodes exhibit more depressed semicircles at high frequencies than CdS-5% GR, indicating that the smaller resistance and more efficient transfer of charge carriers are obtained over the optimal CdS-(GR-M) (M = Ca^{2+}, Cr^{3+}, Mn^{2+}, Fe^{2+}, Co^{2+}, Ni^{2+}, Cu^{2+}, and Zn^{2+}) than those over CdS-5% GR. The EIS results manifest that the addition of metal ions is also able to promote the transfer efficiency of charge carriers across the interface between graphene and semiconductor CdS.

Most recently, the interfacial electron transfer mediator was stepped from metal ions to noble metal palladium (Pd), which can optimize spatial charge carrier transfer across the interface

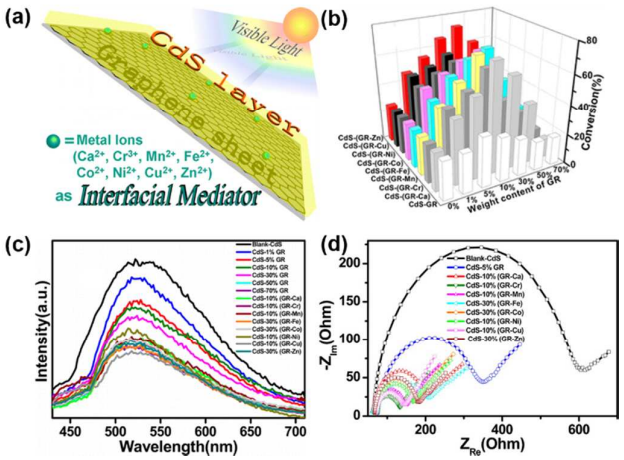

Figure 9. (a) Illustration of metal ions as generic interfacial mediator between CdS and graphene. (b) Photocatalytic performance of blank CdS, CdS–GR, and CdS–(GR–M) (M = Ca^{2+}, Cr^{3+}, Mn^{2+}, Fe^{2+}, Co^{2+}, Ni^{2+}, Cu^{2+}, and Zn^{2+}) nanocomposites with different weight addition ratios of graphene for photocatalytic selective oxidation of benzyl alcohol under visible light (λ > 420 nm) for 2 h. Photoluminescence spectra (c) and electrochemical impedance spectroscopy (EIS) Nyquist diagrams (d) of blank CdS, CdS–GR, and CdS–(GR–M) (M = Ca^{2+}, Cr^{3+}, Mn^{2+}, Fe^{2+}, Co^{2+}, Ni^{2+}, Cu^{2+}, and Zn^{2+}) nanocomposites with different weight addition ratios of graphene. Reprinted with permission from ref.135. Copyright 2014, American Chemical Society.

Nanoscale Accepted Manuscript

between semiconductor (CdS) and graphene.[136] One of the roles of Pd is to serve as electron reservoir to directly trap photogenerated electrons from CdS. Another role is as interfacial mediator to promote electron relay in the ternary CdS–(graphene–Pd) photocatalysts along with conductive graphene as dual co-catalysts. This work substantiates the feasibility of adopting the "interfacial-mediator" strategy to optimize the interfacial charge carriers transfer pathway and efficiency for improved photoactivity of graphene–semiconductor nanocomposites toward target photoredox reactions.

The interfacial contact between graphene and semiconductor can be strengthened by the surface modification. The principle is to assemble semiconductor with graphene by utilizing the electrostatic attraction interaction. After modification of 3-aminopropyltriethoxysilane (APTES) or branched polyethylenimine (BPEI)[109], semiconductors (*e.g.* TiO_2,[46] ZnO,[109] CdS,[137] In_2S_3[138], and $SnNb_2O_6$[109]) are abundant with positively charged amine groups, which provide substantial electrostatic interaction between negatively charged GO or graphene. The enhanced interfacial interaction contributes to the improved photoactivity of graphene-based composite photocatalyst toward different photoredox and photooxidation reactions.

Assembling of graphene into interconnected networks provides efficient 3D transfer pathways for photo-generated electrons, which reduces the recombination rate of electron-hole pairs. Moreover, the hierarchically porous structure can facilitate the mass transfer and offer a large accessible surface area.[139] Zhang *et al.* reported a simple one-step hydrothermal method toward *in situ* growth of ultradispersed mesoporous TiO_2 nanocrystals with (001) facets on 3D porous graphene.[140] This method uses glucose as the dispersant and linker owing to its hierarchically porous structure and high surface area. The strong interaction between TiO_2 and graphene, the facet characteristics, the high electrical conductivity, and the 3D hierarchically porous structure of these composites results in highly active photocatalysis.

5 Summary and Perspectives

Research into graphene-based semiconductor photocatalysts is gaining momentum. Although graphene-based photocatalysts have been widely investigated, key concepts to further enhance the photocatalytic performances show promising opportunities to rationally design graphene-based semiconductor photocatalysts as the next-generation artificial photosynthesis systems with high performance.

Firstly, the band-gap opening of graphene could open a wide scope of graphene for photocatalytic applications. Some strategies have been developed to open up a band-gap in graphene, such as heteroatoms doping,[141] processing graphene sheets into nanoribbons[142] or nanomeshes[143-146]. Among them, doping graphene by nitrogen has been proved to be an effective method for materials engineering toward different photocatalytic applications.[92, 147-155] For example, it was reported that nitrogen-doped graphene (NG) is an excellent support of ZnSe photocatalyst, the as-synthesized composite exhibited remarkably enhanced photocatalytic activities for the bleaching of methyl orange dye under visible-light irradiation.[155] Besides the advantages of better adsorption ability and extended absorption range of light brought by NG, the effect of p-n junctions between NG and ZnSe is another key to improving photoactivity. However, a rational comparison between graphene and NG regarding the improvement of photocatalytic activity is highly sort, which may in turn facilities the utilization of NG for photocatalytic applications.

Secondly, morphology control of graphene-based nanoarchitectures is expected to further improve the photocatalytic performance. The materials engineering should aim to enhance the light absorption, improve the mass transportation, and increase the accessible surface area. For example, the hollow structure may also act as a photon trap-well to allow the multi-scattering of incidence light for the enhancement of light absorption.[59] Thus, more charge carriers can be generated by the incidence photons which will increase the apparent quantum efficiency of photocatalysts.

The advent of robust graphene is sure to make graphene-semiconductor composite photocatalysts promising candidates for solar energy storage and conversion. However, as emphasized by Xu. *et al.,* only by material designing at a system level can we construct the next generation of artificial photocatalytic systems based on graphene-semiconductor photocatalysts with high performance.[17] To be specific, optimizing the structural and electronic properties of each component and enhancing the interfacial electron transfer at the nanoscale simultaneously and harmoniously is critical for the overall photocatalytic activity of graphene-based semiconductor photocatalysts.

Acknowledgements

This original research was proudly supported by the Commonwealth of Australia through the Automotive Australia 2020 Cooperative Research Centre (AutoCRC) and the Fundamental Research Funds for the Central Universities of China (NE2014301).

Notes and references

1. N. Zhang, R. Ciriminna, M. Pagliaro and Y.-J. Xu, *Chem. Soc. Rev.*, 2014, **43**, 5276-5287.
2. S. Liu, Z.-R. Tang, Y. Sun, J. C. Colmenares and Y.-J. Xu, *Chem. Soc. Rev.*, 2015, DOI: 10.1039/C1034CS00408F.
3. K. Nakata and A. Fujishima, *J. Photochem. Photobiol. C: Photochem. Rev.*, 2012, **13**, 169-189.
4. J. Liu, Y. Liu, N. Liu, Y. Han, X. Zhang, H. Huang, Y. Lifshitz, S.-T. Lee, J. Zhong and Z. Kang, *Science*, 2015, **347**, 970-974.
5. M. J. Allen, V. C. Tung and R. B. Kaner, *Chem. Rev.*, 2009, **110**, 132-145.
6. L. Dai, *Acc. Chem. Res.*, 2013, **46**, 31-42.

Nanoscale Accepted Manuscript

This journal is © The Royal Society of Chemistry 20xx

7. R. M. Westervelt, *Science*, 2008, **320**, 324-325.
8. F. Bonaccorso, Z. Sun, T. Hasan and A. C. Ferrari, *Nat Photon*, 2010, **4**, 611-622.
9. E. W. Hill, A. Vijayaragahvan and K. Novoselov, *IEEE Sens J.*, 2011, **11**, 3161-3170.
10. O. Akhavan and E. Ghaderi, *J. Phys. Chem. C*, 2009, **113**, 20214-20220.
11. O. Akhavan, M. Choobtashani and E. Ghaderi, *J. Phys. Chem. C*, 2012, **116**, 9653-9659.
12. O. Akhavan, E. Ghaderi and K. Rahimi, *J. Mater. Chem.*, 2012, **22**, 23260-23266.
13. O. Akhavan and E. Ghaderi, *Nanoscale*, 2013, **5**, 10316-10326.
14. O. Akhavan and E. Ghaderi, *J. Mater. Chem. B*, 2013, **1**, 6291-6301.
15. O. Akhavan, A. Meidanchi, E. Ghaderi and S. Khoei, *J. Mater. Chem. B*, 2014, **2**, 3306-3314.
16. A. Nourmohammadi, R. Rahighi, O. Akhavan and A. Moshfegh, *J. Alloys Compd.*, 2014, **612**, 380-385.
17. M.-Q. Yang, N. Zhang, M. Pagliaro and Y.-J. Xu, *Chem. Soc. Rev.*, 2014, **43**, 8240-8254.
18. M.-Q. Yang and Y.-J. Xu, *Phys. Chem. Chem. Phys.*, 2013, **15**, 19102-19118.
19. N. Zhang, Y. Zhang and Y.-J. Xu, *Nanoscale*, 2012, **4**, 5792-5813.
20. N. Zhang, Y. Zhang, M.-Q. Yang and Y.-J. Xu, *Curr. Org. Chem.*, 2013, **17**, 2503-2515.
21. Q. Xiang, J. Yu and M. Jaroniec, *Chem. Soc. Rev.*, 2012, **41**, 782-796.
22. G. Xie, K. Zhang, B. Guo, Q. Liu, L. Fang and J. R. Gong, *Adv. Mater.*, 2013, **25**, 3820-3839.
23. A. K. Geim and I. V. Grigorieva, *Nature*, 2013, **499**, 419-425.
24. Y. Zhang, Z.-R. Tang, X. Fu and Y.-J. Xu, *ACS Nano*, 2011, **5**, 7426-7435.
25. A. L. Linsebigler, G. Lu and J. T. Yates, *Chem. Rev.*, 1995, **95**, 735-758.
26. J. Soria, J. C. Conesa, V. Augugliaro, L. Palmisano, M. Schiavello and A. Sclafani, *J. Phys. Chem.*, 1991, **95**, 274-282.
27. K. S. Novoselov, A. K. Geim, S. V. Morozov, D. Jiang, Y. Zhang, S. V. Dubonos, I. V. Grigorieva and A. A. Firsov, *Science*, 2004, **306**, 666-669.
28. M. D. Stoller, S. Park, Y. Zhu, J. An and R. S. Ruoff, *Nano Lett.*, 2008, **8**, 3498-3502.
29. R. R. Nair, P. Blake, A. N. Grigorenko, K. S. Novoselov, T. J. Booth, T. Stauber, N. M. R. Peres and A. K. Geim, *Science*, 2008, **320**, 1308.
30. C. Lee, X. Wei, J. W. Kysar and J. Hone, *Science*, 2008, **321**, 385-388.
31. A. A. Balandin, S. Ghosh, W. Bao, I. Calizo, D. Teweldebrhan, F. Miao and C. N. Lau, *Nano Lett.*, 2008, **8**, 902-907.
32. Y. Zhang, Z.-R. Tang, X. Fu and Y.-J. Xu, *ACS Nano*, 2010, **4**, 7303-7314.
33. N. Zhang, Y. Zhang, M.-Q. Yang, Z.-R. Tang and Y.-J. Xu, *J. Catal.*, 2013, **299**, 210-221.
34. W. S. Hummers and R. E. Offeman, *J. Am. Chem. Soc.*, 1958, **80**, 1339.
35. M. S. A. Sher Shah, A. R. Park, K. Zhang, J. H. Park and P. J. Yoo, *ACS Appl. Mater. Interfaces*, 2012, **4**, 3893-3901.
36. A. Cao, Z. Liu, S. Chu, M. Wu, Z. Ye, Z. Cai, Y. Chang, S. Wang, Q. Gong and Y. Liu, *Adv. Mater.*, 2010, **22**, 103-106.
37. I. Y. Kim, J. M. Lee, T. W. Kim, H. N. Kim, H.-i. Kim, W. Choi and S.-J. Hwang, *Small*, 2012, **8**, 1038-1048.
38. G. Williams, B. Seger and P. V. Kamat, *ACS Nano*, 2008, **2**, 1487-1491.
39. O. Akhavan, M. Abdolahad, A. Esfandiar and M. Mohatashamifar, *J. Phys. Chem. C*, 2010, **114**, 12955-12959.
40. G. Williams and P. V. Kamat, *Langmuir*, 2009, **25**, 13869-13873.
41. O. Akhavan, *Carbon*, 2011, **49**, 11-18.
42. X. Xie, Z. Ao, D. Su, J. Zhang and G. Wang, *Adv. Funct. Mater.*, 2015, **25**, 1393-1403.
43. K. P. Loh, Q. Bao, G. Eda and M. Chhowalla, *Nat. Chem.*, 2010, **2**, 1015-1024.
44. M.-Q. Yang, X. Pan, N. Zhang and Y.-J. Xu, *CrystEngComm*, 2013, **15**, 6819-6828.
45. Y. Zhang, N. Zhang, Z.-R. Tang and Y.-J. Xu, *J. Phys. Chem. C*, 2014, **118**, 5299-5308.
46. H. Zhang, X. Lv, Y. Li, Y. Wang and J. Li, *ACS Nano*, 2009, **4**, 380-386.
47. X.-Y. Zhang, H.-P. Li, X.-L. Cui and Y. Lin, *J. Mater. Chem.*, 2010, **20**, 2801-2806.
48. J. Guo, S. Zhu, Z. Chen, Y. Li, Z. Yu, Q. Liu, J. Li, C. Feng and D. Zhang, *Ultrason. Sonochem.*, 2011, **18**, 1082-1090.
49. Y. Liang, H. Wang, H. Sanchez Casalongue, Z. Chen and H. Dai, *Nano Res.*, 2010, **3**, 701-705.
50. N. Li, G. Liu, C. Zhen, F. Li, L. Zhang and H.-M. Cheng, *Adv. Funct. Mater.*, 2011, **21**, 1717-1722.
51. J. Liu, H. Bai, Y. Wang, Z. Liu, X. Zhang and D. D. Sun, *Adv. Funct. Mater.*, 2010, **20**, 4175-4181.
52. P. Dong, Y. Wang, L. Guo, B. Liu, S. Xin, J. Zhang, Y. Shi, W. Zeng and S. Yin, *Nanoscale*, 2012, **4**, 4641-4649.
53. X. Zhang, Y. Sun, X. Cui and Z. Jiang, *Int. J. Hydrogen Energy*, 2012, **37**, 811-815.
54. Q. Zhai, B. Tang and G. Hu, *J. Hazard. Mater.*, 2011, **198**, 78-86.
55. W. Tu, Y. Zhou, Q. Liu, S. Yan, S. Bao, X. Wang, M. Xiao and Z. Zou, *Adv. Funct. Mater.*, 2013, **23**, 1743-1749.
56. K. K. Manga, Y. Zhou, Y. Yan and K. P. Loh, *Adv. Funct. Mater.*, 2009, **19**, 3638-3643.
57. J. Du, X. Lai, N. Yang, J. Zhai, D. Kisailus, F. Su, D. Wang and L. Jiang, *ACS Nano*, 2010, **5**, 590-596.
58. H.-I. Kim, G.-H. Moon, D. Monllor-Satoca, Y. Park and W. Choi, *J. Phys. Chem. C*, 2011, **116**, 1535-1543.
59. W. Tu, Y. Zhou, Q. Liu, Z. Tian, J. Gao, X. Chen, H. Zhang, J. Liu and Z. Zou, *Adv. Funct. Mater.*, 2012, **22**, 1215-1221.
60. Y. Zhang, N. Zhang, Z.-R. Tang and Y.-J. Xu, *Phys. Chem. Chem. Phys.*, 2012, **14**, 9167-9175.
61. Q. Xiang, J. Yu and M. Jaroniec, *Nanoscale*, 2011, **3**, 3670-3678.
62. B. Liu, Y. Huang, Y. Wen, L. Du, W. Zeng, Y. Shi, F. Zhang, G. Zhu, X. Xu and Y. Wang, *J. Mater. Chem.*, 2012, **22**, 7484-7491.
63. W.-S. Wang, D.-H. Wang, W.-G. Qu, L.-Q. Lu and A.-W. Xu, *J. Phys. Chem. C*, 2012, **116**, 19893-19901.

Nanoscale Accepted Manuscript

64. Z. Wang, B. Huang, Y. Dai, Y. Liu, X. Zhang, X. Qin, J. Wang, Z. Zheng and H. Cheng, *CrystEngComm*, 2012, **14**, 1687-1692.
65. C. Wang, D. Meng, J. Sun, J. Memon, Y. Huang and J. Geng, *Adv. Mater. Interfaces*, 2014, **1**, 1300150.
66. Z. Zhang, F. Xiao, Y. Guo, S. Wang and Y. Liu, *ACS Appl. Mater. Interfaces*, 2013, **5**, 2227-2233.
67. X. Cao, G. Tian, Y. Chen, J. Zhou, W. Zhou, C. Tian and H. Fu, *J. Mater. Chem. A*, 2014, **2**, 4366-4374.
68. Q. Li, B. Guo, J. Yu, J. Ran, B. Zhang, H. Yan and J. R. Gong, *J. Am. Chem. Soc.*, 2011, **133**, 10878-10884.
69. S. Park, K.-S. Lee, G. Bozoklu, W. Cai, S. T. Nguyen and R. S. Ruoff, *ACS Nano*, 2008, **2**, 572-578.
70. X. Pan, M.-Q. Yang and Y.-J. Xu, *Phys. Chem. Chem. Phys.*, 2014, **16**, 5589-5599.
71. X. Xie, D. Su, S. Chen, J. Zhang, S. Dou and G. Wang, *Chem. - Asian J.*, 2014, **9**, 1611-1617.
72. J. Zhang, Z. Xiong and X. S. Zhao, *J. Mater. Chem.*, 2011, **21**, 3634-3640.
73. C. Zhu, P. Wang, L. Wang, L. Han and S. Dong, *Nanoscale*, 2011, **3**, 4376-4382.
74. S. Humaira, K. C. Kemp, C. Vimlesh and S. K. Kwang, *Nanotechnology*, 2012, **23**, 355705.
75. B. Li, T. Liu, Y. Wang and Z. Wang, *J. Colloid Interface Sci.*, 2012, **377**, 114-121.
76. T. Xu, L. Zhang, H. Cheng and Y. Zhu, *Appl. Catal. B: Environ.*, 2011, **101**, 382-387.
77. Y. Liu, Y. Hu, M. Zhou, H. Qian and X. Hu, *Appl. Catal. B: Environ.*, 2012, **125**, 425-431.
78. P. D. Tran, S. K. Batabyal, S. S. Pramana, J. Barber, L. H. Wong and S. C. J. Loo, *Nanoscale*, 2012, **4**, 3875-3878.
79. K. Morishige and T. Hamada, *Langmuir*, 2005, **21**, 6277-6281.
80. D. Wang, R. Kou, D. Choi, Z. Yang, Z. Nie, J. Li, L. V. Saraf, D. Hu, J. Zhang, G. L. Graff, J. Liu, M. A. Pope and I. A. Aksay, *ACS Nano*, 2010, **4**, 1587-1595.
81. S. Chen, J. Zhu, X. Wu, Q. Han and X. Wang, *ACS Nano*, 2010, **4**, 2822-2830.
82. S. Liu, J. Tian, L. Wang, Y. Luo and X. Sun, *Catal. Sci. Technol.*, 2012, **2**, 339-344.
83. N. Zhang, Y. Zhang, X. Pan, X. Fu, S. Liu and Y.-J. Xu, *J. Phys. Chem. C*, 2011, **115**, 23501-23511.
84. N. Zhang, Y. Zhang, X. Pan, M.-Q. Yang and Y.-J. Xu, *J. Phys. Chem. C*, 2012, **116**, 18023-18031.
85. Z. Gao, N. Liu, D. Wu, W. Tao, F. Xu and K. Jiang, *Appl. Surf. Sci.*, 2012, **258**, 2473-2478.
86. P. Gao, J. Liu, S. Lee, T. Zhang and D. D. Sun, *J. Mater. Chem.*, 2012, **22**, 2292-2298.
87. X. Liu, L. Pan, T. Lv, G. Zhu, Z. Sun and C. Sun, *Chem. Commun.*, 2011, **47**, 11984-11986.
88. X. An, J. C. Yu, F. Wang, C. Li and Y. Li, *Appl. Catal. B: Environ.*, 2013, **129**, 80-88.
89. Y. Zhang, J. Tian, H. Li, L. Wang, X. Qin, A. M. Asiri, A. O. Al-Youbi and X. Sun, *Langmuir*, 2012, **28**, 12893-12900.
90. L. Yuan, M.-Q. Yang and Y.-J. Xu, *J. Mater. Chem. A*, 2014, **2**, 14401-14412.
91. J. Zhang, J. Yu, M. Jaroniec and J. R. Gong, *Nano Lett.*, 2012, **12**, 4584-4589.
92. F. Meng, J. Li, S. K. Cushing, M. Zhi and N. Wu, *J. Am. Chem. Soc.*, 2013, **135**, 10286-10289.
93. E. Gao, W. Wang, M. Shang and J. Xu, *Phys. Chem. Chem. Phys.*, 2011, **13**, 2887-2893.
94. H. Ma, J. Shen, M. Shi, X. Lu, Z. Li, Y. Long, N. Li and M. Ye, *Appl. Catal. B: Environ.*, 2012, **121–122**, 198-205.
95. Y. Fu, X. Sun and X. Wang, *Mater. Chem. Phys.*, 2011, **131**, 325-330.
96. F. Zhou, R. Shi and Y. Zhu, *J. Mol. Catal. A: Chem.*, 2011, **340**, 77-82.
97. P. Wang, Y. Ao, C. Wang, J. Hou and J. Qian, *Carbon*, 2012, **50**, 5256-5264.
98. A. Mukherji, B. Seger, G. Q. Lu and L. Wang, *ACS Nano*, 2011, **5**, 3483-3492.
99. Y. Fu and X. Wang, *Ind. Eng. Chem. Res.*, 2011, **50**, 7210-7218.
100. Y. Fu, P. Xiong, H. Chen, X. Sun and X. Wang, *Ind. Eng. Chem. Res.*, 2011, **51**, 725-731.
101. Y. Fu, H. Chen, X. Sun and X. Wang, *Appl. Catal. B: Environ.*, 2012, **111–112**, 280-287.
102. X. Zhang, X. Chang, M. A. Gondal, B. Zhang, Y. Liu and G. Ji, *Appl. Surf. Sci.*, 2012, **258**, 7826-7832.
103. X. Tu, S. Luo, G. Chen and J. Li, *Chem.—Eur. J.*, 2012, **18**, 14359-14366.
104. Z. Liu, W. Xu, J. Fang, X. Xu, S. Wu, X. Zhu and Z. Chen, *Appl. Surf. Sci.*, 2012, **259**, 441-447.
105. Y. Min, F.-J. Zhang, W. Zhao, F. Zheng, Y. Chen and Y. Zhang, *Chem. Eng. J.*, 2012, **209**, 215-222.
106. C. Wu, Y. Zhang, S. Li, H. Zheng, H. Wang, J. Liu, K. Li and H. Yan, *Chem. Eng. J.*, 2011, **178**, 468-474.
107. X. Bai, L. Wang and Y. Zhu, *ACS Catal.*, 2012, **2**, 2769-2778.
108. X. Zhang, X. Quan, S. Chen and H. Yu, *Appl. Catal. B: Environ.*, 2011, **105**, 237-242.
109. L. Yuan, M.-Q. Yang and Y.-J. Xu, *Nanoscale*, 2014, **6**, 6335-6345.
110. L. Liu, J. Liu and D. D. Sun, *Catal. Sci. Technol.*, 2012, **2**, 2525-2532.
111. Y. Zhang, N. Zhang, Z.-R. Tang and Y.-J. Xu, *ACS Nano*, 2012, **6**, 9777-9789.
112. Q. Xiang, J. Yu and M. Jaroniec, *J. Phys. Chem. C*, 2011, **115**, 7355-7363.
113. J. Hou, Z. Wang, W. Kan, S. Jiao, H. Zhu and R. V. Kumar, *J. Mater. Chem.*, 2012, **22**, 7291-7299.
114. S. Sakthivel and H. Kisch, *Angew. Chem., Int. Ed.*, 2003, **42**, 4908-4911.
115. G. Jiang, Z. Lin, C. Chen, L. Zhu, Q. Chang, N. Wang, W. Wei and H. Tang, *Carbon*, 2011, **49**, 2693-2701.
116. C. Hou, Q. Zhang, Y. Li and H. Wang, *J. Hazard. Mater.*, 2012, **205–206**, 229-235.
117. X. Pan, Y. Zhao, S. Liu, C. L. Korzeniewski, S. Wang and Z. Fan, *ACS Appl. Mater. Interfaces*, 2012, **4**, 3944-3950.
118. S. D. Perera, R. G. Mariano, K. Vu, N. Nour, O. Seitz, Y. Chabal and K. J. Balkus, *ACS Catal.*, 2012, **2**, 949-956.
119. A. Du, Y. H. Ng, N. J. Bell, Z. Zhu, R. Amal and S. C. Smith, *J. Phys. Chem. Lett.*, 2011, **2**, 894-899.

Nanoscale Accepted Manuscript

This journal is © The Royal Society of Chemistry 20xx

120. J. T. Robinson, S. M. Tabakman, Y. Liang, H. Wang, H. Sanchez Casalongue, D. Vinh and H. Dai, *J. Am. Chem. Soc.*, 2011, **133**, 6825-6831.
121. C. Han, Z. Chen, N. Zhang, J. C. Colmenares and Y.-J. Xu, *Adv. Funct. Mater.*, 2015, **25**, 221-229.
122. N. Yang, Y. Liu, H. Wen, Z. Tang, H. Zhao, Y. Li and D. Wang, *ACS Nano*, 2013, **7**, 1504-1512.
123. B. Weng, J. Wu, N. Zhang and Y.-J. Xu, *Langmuir*, 2014, **30**, 5574-5584.
124. F.-X. Xiao, J. Miao and B. Liu, *J. Am. Chem. Soc.*, 2014, **136**, 1559-1569.
125. A. Iwase, Y. H. Ng, Y. Ishiguro, A. Kudo and R. Amal, *J. Am. Chem. Soc.*, 2011, **133**, 11054-11057.
126. F. Meng, J. Li, S. K. Cushing, J. Bright, M. Zhi, J. D. Rowley, Z. Hong, A. Manivannan, A. D. Bristow and N. Wu, *ACS Catal.*, 2013, **3**, 746-751.
127. Z. Chen, N. Zhang and Y.-J. Xu, *CrystEngComm*, 2013, **15**, 3022-3030.
128. Y. Zhang, Z. Chen, S. Liu and Y.-J. Xu, *Appl. Catal. B: Environ.*, 2013, **140–141**, 598-607.
129. B. Weng, M.-Q. Yang, N. Zhang and Y.-J. Xu, *J. Mater. Chem. A*, 2014, **2**, 9380-9389.
130. C. Han, M.-Q. Yang, B. Weng and Y.-J. Xu, *Phys. Chem. Chem. Phys.*, 2014, **16**, 16891-16903.
131. X. Yang, H. Cui, Y. Li, J. Qin, R. Zhang and H. Tang, *ACS Catal.*, 2013, **3**, 363-369.
132. X. Guo, C. Hao, G. Jin, H.-Y. Zhu and X.-Y. Guo, *Angew. Chem., Int. Ed.*, 2014, **53**, 1973-1977.
133. Q. Huang, S. Tian, D. Zeng, X. Wang, W. Song, Y. Li, W. Xiao and C. Xie, *ACS Catal.*, 2013, **3**, 1477-1485.
134. Y. T. Liang, B. K. Vijayan, K. A. Gray and M. C. Hersam, *Nano Lett.*, 2011, **11**, 2865-2870.
135. N. Zhang, M.-Q. Yang, Z.-R. Tang and Y.-J. Xu, *ACS Nano*, 2014, **8**, 623-633.
136. C. Han, M.-Q. Yang, N. Zhang and Y.-J. Xu, *J. Mater. Chem. A*, 2014, **2**, 19156-19166.
137. S. Liu, Z. Chen, N. Zhang, Z.-R. Tang and Y.-J. Xu, *J. Phys. Chem. C*, 2013, **117**, 8251-8261.
138. M.-Q. Yang, B. Weng and Y.-J. Xu, *Langmuir*, 2013, **29**, 10549-10558.
139. X. Xie, S. Chen, B. Sun, C. Wang and G. Wang, *ChemSusChem*, 2015, DOI: 10.1002/cssc.201500149.
140. B. Qiu, M. Xing and J. Zhang, *J. Am. Chem. Soc.*, 2014, **136**, 5852-5855.
141. D. Wei, Y. Liu, Y. Wang, H. Zhang, L. Huang and G. Yu, *Nano Lett.*, 2009, **9**, 1752-1758.
142. V. Barone, O. Hod and G. E. Scuseria, *Nano Lett.*, 2006, **6**, 2748-2754.
143. J. Bai, X. Zhong, S. Jiang, Y. Huang and X. Duan, *Nature Nanotech.*, 2010, **5**, 190-194.
144. O. Akhavan, *ACS Nano*, 2010, **4**, 4174-4180.
145. O. Akhavan and E. Ghaderi, *Small*, 2013, **9**, 3593-3601.
146. O. Akhavan, E. Ghaderi and S. A. Shirazian, *Colloids Surf. B: Biointerfaces*, 2015, **126**, 313-321.
147. L. S. Panchakarla, K. S. Subrahmanyam, S. K. Saha, A. Govindaraj, H. R. Krishnamurthy, U. V. Waghmare and C. N. R. Rao, *Adv. Mater.*, 2009, **21**, 4726-4730.
148. X. Xie, J. Long, J. Xu, L. Chen, Y. Wang, Z. Zhang and X. Wang, *RSC Adv.*, 2012, **2**, 12438-12446.
149. M. Latorre-Sánchez, A. Primo and H. García, *Angew. Chem., Int. Ed.*, 2013, **52**, 11813-11816.
150. U. Maitra, U. Gupta, M. De, R. Datta, A. Govindaraj and C. N. R. Rao, *Angew. Chem., Int. Ed.*, 2013, **52**, 13057-13061.
151. L. He, L. Jing, Y. Luan, L. Wang and H. Fu, *ACS Catal.*, 2014, **4**, 990-998.
152. Z. Mou, Y. Wu, J. Sun, P. Yang, Y. Du and C. Lu, *ACS Appl. Mater. Interfaces*, 2014, **6**, 13798-13806.
153. M. Xing, X. Li and J. Zhang, *Sci. Rep.*, 2014, **4**, 5493.
154. T.-F. Yeh, C.-Y. Teng, S.-J. Chen and H. Teng, *Adv. Mater.*, 2014, **26**, 3297-3303.
155. P. Chen, T.-Y. Xiao, H.-H. Li, J.-J. Yang, Z. Wang, H.-B. Yao and S.-H. Yu, *ACS Nano*, 2011, **6**, 712-719.

Nanoscale Accepted Manuscript